ChemPubSoc Europe

DOI: 10.1002/open.201900186

Open Access ChemistryOPEN Full Papers

Creation of Conductive Graphene Materials by Bacterial Reduction Using *Shewanella Oneidensis*

Benjamin A. E. Lehner,[c] Vera A. E. C. Janssen,[d] Ewa M. Spiesz,[c] Dominik Benz,[e] Stan J. J. Brouns,[c] Anne S. Meyer,*[b] and Herre S. J. van der Zant*[a]

Graphene's maximized surface-to-volume ratio, high conductance, mechanical strength, and flexibility make it a promising nanomaterial. However, large-scale graphene production is typically cost-intensive. This manuscript describes a microbial reduction approach for producing graphene that utilizes the bacterium *Shewanella oneidensis* in combination with modern nanotechnology to enable a low-cost, large-scale production method. The bacterial reduction approach presented in this paper increases the conductance of single graphene oxide flakes as well as bulk graphene oxide sheets by 2.1 to 2.7 orders of magnitude respectively while simultaneously retaining a high surface-area-to-thickness ratio. *Shewanella*-mediated reduction was employed in conjunction with electron-beam lithography to reduce one surface of individual graphene oxide flakes. This methodology yielded conducting flakes with differing functionalization on the top and bottom faces. Therefore, microbial reduction of graphene oxide enables the development and up-scaling of new types of graphene-based materials and devices with a variety of applications including nano-composites, conductive inks, and biosensors, while avoiding usage of hazardous, environmentally-unfriendly chemicals.

1. Introduction

Pristine graphene was the first two-dimensional material to be identified.[1] The one-atom thickness of single-layer graphene gives it the highest possible surface-to-volume ratio and 97% optical transparency.[2] Its electrical conductivity of up to 10^8 S/m and thermal conductivity of 4800 to 5300 W/mK are superior to those of the most conductive elements (i.e., silver, gold and copper).[3,4] Additionally, the Young's modulus of 1 TPa and intrinsic strength of 130 GPa identify graphene as the strongest measured material to date.[5] These exceptional properties have led to various applications for graphene in bioanalytics, drug carriers, composite materials, improved transistors, batteries, hydrogen storage, and photocatalysis, among others.[6–14] However, the primary hurdle to the widespread usage of graphene-based materials is the lack of reliable, clean, cost-efficient, and scalable graphene production.

The two predominant production methods for graphene are chemical vapor deposition (CVD) and exfoliation of graphite. CVD set-ups utilize a substrate material (e.g. copper) onto which methane is deposited, forming single-layer graphene. Their major drawbacks are the limited surface area of the substrate, the need for a specialized atmosphere for graphene growth, and difficulties in removing the grown graphene from the substrate.[15] While the quality of CVD-produced graphene is typically high, industrial up-scaling is challenging and expensive.[16,17] Methodologies for exfoliation of graphite are diverse, but one promising technique for scalable production is the oxidation and exfoliation of graphite to graphene oxide (GO), followed by its subsequent reduction to graphene (Figure 1).[14,18–20] The production of graphite oxide and its exfoliation to GO can be performed using synthetic chemistry and have been demonstrated to be scalable as well as cost-efficient.[18,19,21] In contrast, the reduction of GO to graphene often involves the usage of harsh chemistry (e.g. hydrazine), which can add undesired nitrogen groups onto the surface, has very high energy demands, and can cause π-π stacking of the freshly-produced layers of reduced graphene oxide, removing the advantageous properties that result from the two-dimensionality of graphene.[14,22,23]

One intriguing possibility to reduce graphene oxide in a more sustainable, easily up-scalable, and cost-efficient way is via the metal-oxide-reducing bacterium *Shewanella*

[a] *Prof. Dr. H. S. J. van der Zant*
Department of Quantum Nanoscience
Delft University of Technology
Lorentzweg 1, 2628 CJ Delft, Netherlands
Tel.: +31-15-278-7733
E-mail: H.S.J.vanderZant@tudelft.nl
[b] *Dr. A. S. Meyer*
Department of Biology
University of Rochester
Rochester, NY, 14627, United States of America
Tel: +1-585-275-9290
E-mail: anne@annemeyerlab.org
[c] *B. A. E. Lehner, Dr. E. M. Spiesz, Dr. S. J. J. Brouns*
Department of Bionanoscience
Delft University of Technology
Van der Maasweg 9, 2629 HZ Delft, The Netherlands
[d] *V. A. E. C. Janssen*
Department of Quantum Nanoscience
Delft University of Technology
Lorentzweg 1, 2628 CJ Delft, Netherlands
[e] *D. Benz*
Department of Chemical Engineering
Delft University of Technology
Van der Maasweg 9, 2629 HZ Delft, The Netherlands

Supporting information for this article is available on the WWW under https://doi.org/10.1002/open.201900186

© 2019 The Authors. Published by Wiley-VCH Verlag GmbH & Co. KGaA. This is an open access article under the terms of the Creative Commons Attribution Non-Commercial License, which permits use, distribution and reproduction in any medium, provided the original work is properly cited and is not used for commercial purposes.

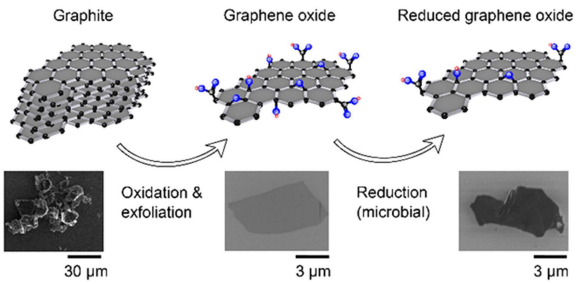

Figure 1. Schematic overview of the generation of reduced graphene oxide by oxidizing and exfoliating graphite to form graphene oxide (GO), which is then reduced to produce reduced graphene oxide (rGO). Grey hexagons represent the carbon back-bone, the blue dots represent oxygen, and the red dots represent hydrogen. Scanning Electron Microscopy (SEM) images obtained of flakes extracted from the bulk solution are included to illustrate each step.

oneidensis.[24–26] *S. oneidensis* has evolved to use inorganic materials as an electron acceptor during anaerobic respiration..[27] *S. oneidensis* can deliver electrons to inorganic acceptor materials both by electron shuttles and via direct surface-to-surface contact mediated by its Mtr respiratory pathway, which consists of multiple different proteins which pass electrons from the bacterial cytoplasm, through the cell membranes, and up to the surface of the bacterium.[25,26] When graphene oxide is provided, the electrons from *S. oneidensis* react with the oxygen groups of the graphene oxide, leading to a restoration of the sp^2 orbitals forming the characteristic hexagonal lattice of graphene. Graphene oxide contains epoxyl, carboxyl, and hydroxyl groups both on the upper and lower surfaces of the flakes.[14] These groups have different binding energies, and it is not yet known which of those groups can be reduced by *Shewanella oneidensis*.

The bacterial mechanism of GO reduction avoids harsh chemicals and could potentially be upscaled using bioreactors.[24–26] However, the conductivity of single flakes, the average thickness after reduction, and the structural quality of microbially-reduced graphene oxide (mrGO) have not yet been determined, making it impossible to identify the feasibility of the microbial production approach and the range of potential applications for reduced graphene oxide produced through this method. A high conductance and surface-to-volume ratio would make mrGO applicable to field effect transistors (FET), biosensors, transparent conductors, batteries, graphene polymer nanocomposites, and conductive inks.[28–33]

Thorough characterization of the conductive properties of mrGO requires a combination of single-flake measurements, to identify the intrinsic resistance within flakes, and bulk measurements, to evaluate the effectiveness of interflake charge movement. In this study, we combined for the first time conductance measurements of microbially-reduced flakes with determination of their surface-area-to-thickness ratio and compared them to GO and chemically-reduced graphene oxide (crGO). Our analyses indicate that microbial reduction of a GO suspension produces a 2.5 orders-of-magnitude increase in conductance, with no significant change in the flake thickness. X-ray photoelectron spectroscopy (XPS) analysis of the microbially-reduced graphene oxide revealed that C–O(H) hydroxyl bonds were strongly influenced by the bacterial reduction, while C=O groups were not affected, in dramatic contrast to the chemically-reduced GO. The flake thickness of mrGO was shown to be significantly lower than in crGO and remained constant over a two-week storage period, which is essential for bioink and biosensor applications. By combining the reduction capabilities of *Shewanella oneidensis* with electron-beam lithography a completely new methodology was developed to functionalize the surfaces of single graphene oxide flakes on only one side, which could improve the selectivity of biosensors or tune the structural properties of nanocomposites.

2. Results and Discussion

2.1. Microbial Reduction of Graphene Oxide

In order to produce microbially-reduced graphene oxide, graphite was first oxidized and exfoliated to graphite oxide via an optimized Hummer and Offeman method (Figure 1).[19,21] Graphite oxide production was monitored via a color change from black to yellow (Figure 2A). The multi-layered graphite oxide stacks were sonicated and filtered to obtain one-layer to few-layer flakes of graphene oxide (Figure 1). The resultant flakes were then incubated with *S. oneidensis* in rich growth medium under either aerobic or anaerobic conditions (Figure 2B), and reduction to mrGO was observed via the reverse color change from yellow to black (Figure 2A) and continuous optical density measurement ($O.D._{600}$) using a UV-VIS Spectrometer at 600 nm (Figure 2C).

To compare the degree of reduction, the average absorbance due to the growth of bacteria under the same conditions ($n=9$) and the baseline absorbance of graphene oxide were subtracted (Figure 2D). Both the aerobic and anaerobic conditions for microbial reduction yielded a robust increase in the amount of rGO, which plateaued after 30 hours. The aerobic reduction initially displayed a lag phase, potentially because of the usage of oxygen as additional electron acceptor. There was no significant difference between the amount of rGO production under aerobic vs. anaerobic conditions after 48 hours (Students T-test two-tailed, two samples with equal variance, $p=0.52$, $n=6$). A colony forming unit (CFU) assay was performed to assess the toxicity of GO for *Shewanella oneidensis*. No harmful effects on the growth of the bacteria in presence of graphene oxide were found (Figure S1).

Additional tests utilizing a minimal growth medium and additional added carbon sources (lactate and fumarate) were conducted but did not result in a more efficient reduction of GO. For all further experiments, we performed microbial reduction using a rich growth medium in an aerobic environment (schematically shown in Figure 2B), due to the ease and inexpensiveness of the procedure.

To determine the quality of the reduced GO samples, the chemical properties of the graphene derivatives were analyzed following the reduction of graphene oxide utilizing *S. oneidensis* (for mrGO) or hydrazine (for crGO). The reduction efficiency

© 2019 The Authors. Published by Wiley-VCH Verlag GmbH & Co. KGaA

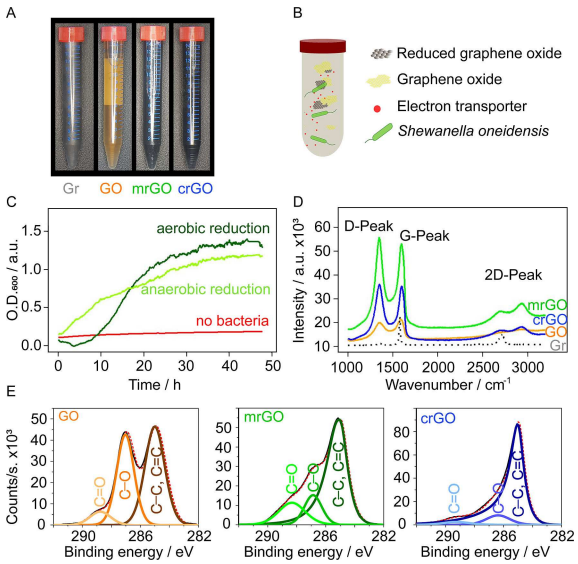

Figure 2. Chemical analyses of microbially- and chemically-reduced graphene oxide. (A) Change of optical properties during generation of reduced graphene oxide. Samples are, from left to right, graphite (Gr), graphene oxide (GO), microbially-reduced graphene oxide (mrGO), and chemically-reduced graphene oxide (crGO). (B) Schematic of microbial graphene oxide reduction. *Shewanella* bacteria perform reduction of graphene oxide flakes at room temperature in liquid medium via direct reduction as well as reduction through secreted electron transporter molecules. (C) Production of reduced graphene oxide over time for aerobic (dark green) and anaerobic (light green) microbial reduction in TSB growth medium, measured via optical density at 600 nm. The $O.D._{600}$ values of a sample containing only *Shewanella* bacteria in TSB and the baseline $O.D._{600}$ value of a sample containing only graphene oxide have been subtracted from each data set. A no-bacteria control, composed of only graphene oxide in TSB is shown in red. (D) Raman spectra of graphite (black), graphene oxide (orange), microbially-reduced graphene oxide (green), and chemically-reduced graphene oxide (blue). Reduction of graphene oxide is indicated by changes in the ratio between the G peak and the D peak as well as a slight shift of the G peak wavenumbers. (E) X-Ray Photoelectron Spectroscopy (XPS) of graphene oxide (left), microbially-reduced graphene oxide (middle), and chemically-reduced graphene oxide (right).

(carbon/oxygen ratio) and the amount of defects were determined, since these properties contribute substantially to the emergent electrical and physical properties of graphene materials.[22] We used Raman spectroscopy to evaluate the status of the sp^2 and sp^3 orbitals in the GO, mrGO, and crGO samples. The amounts of defects in graphene can be estimated via the ratio of the intensities of the D peak and the G peak in the Raman spectrum, (I(D)/I(G)), as well as the width of these peaks.[34] The G peak results from in-plane vibrations primarily from sp^2 hybridization characteristic of highly-ordered materials such as graphene or graphite, while out-of-plane vibrations due to structural defects or sp^3 bonds resulting from oxygen binding are the main contributor to the D peak.[35] After oxidation, both peaks became wider due to the increased amount of disorder in comparison to graphite (Gr vs. GO, Figure 2D).[36] Oxidation also resulted in an increase in the I(D)/I(G) ratio, apparently due to a decreased contribution of in-plane vibrations (G-peak), as well as oxygen binding to the carbon lattice, which caused increased out-of-plane vibrations (D-peak). The I(D)/I(G) ratio continued to increase upon chemical as well as microbial reduction. This change can be attributed to the formation of new sp^2 domains increasing the number of graphene-like domains.[37]

For mrGO, we obtained an I(D)/(I(G) ratio of 1.00 ± 0.09 ($n = 4$), which was not significantly different from the I(D)/(I(G) ratio measured for crGO (1.00 ± 0.03, $n = 4$, $p = 0.79$). Both values were 15% larger and significantly different from the I(D)/(I(G) ratio obtained for GO (0.85 ± 0.03, $n = 4$) (One-way ANOVA with Tukey PostHoc test, p-values: GO-mrGO = 0.049, GO-crGO = 0.012, $n = 4$), indicating a decreased amount of defects in the microbially-reduced GO samples in comparison to GO.

As the number of layers, as well as wrinkles and multiple types of defects in the lattice, may contribute to the D peak in graphene materials, the I(D)/I(G) ratio is a less reliable indicator to quantify the grade of reduction.[38] X-Ray photoelectron spectroscopy (XPS) allows for a better quantification of reduction as well as the identification of the elemental composition and the chemical states in the sample (i.e. C–C and C=C bonds vs. C–O bonds or C=O bonds) of mrGO in comparison to crGO and GO (Figure 2E). The atomic percentage (atomic %), calculated via the peak area, of C–C and C=C bonds, was 32.7 ± 1.0% for GO and increased to 48.0 ± 1.0% in mrGO and 72.9 ± 1.0% in crGO. This percentage increase in carbon bonds was caused by the removal of oxygen during the reduction processes. Accordingly, the peak area of C–O and C=O bonds was 31.6 ± 0.2% for GO and decreased to 22.5 ± 2.0% for mrGO and 11.8 ± 1.2% for crGO. The data also showed that the peak area (in atomic %) of C=O bonds was not affected by microbial reduction (5.6 ± 0.3% GO and 6.4 ± 1.9% in mrGO) but decreased after chemical reduction (0.7 ± 0.7% in crGO).[17,25]

2.2. Conductive Characterization of Microbially-Reduced Graphene Oxide

To quantify the electronic properties of our microbially-reduced GO, we measured the current as a function of bias voltage (I–V curves) of bulk samples (Figure 3A) as well as of single flakes (Figure 3B, C, D). For the bulk conductance measurements, GO, mrGO, and crGO were deposited onto non-conductive filter paper. Microbial reduction caused an average increase in the current of 2.1 orders of magnitude, and chemical reduction caused an increase of 3.2 orders of magnitude at the same bias voltage. The conductances of these bulk samples are directly comparable because the samples share the same physical dimensions. The conductance of graphene materials in a bulk ensemble can arise from electrons travelling either within single flakes or due to flake-to-flake transport. To understand the role of charge carrier movement between flakes versus charge movement within our GO flakes, single-flake conductances were measured. Single flakes of GO, mrGO, and crGO were deposited onto a Si/SiO_2 chip (Figure 3B). Atomic force microscopy (AFM) measurements were performed to obtain geometrical data for the individual flakes (thickness, width, and length), in order to compensate for differing flake geometries. The I–V curves of flakes with similar geometry (a length-to-

© 2019 The Authors. Published by Wiley-VCH Verlag GmbH & Co. KGaA

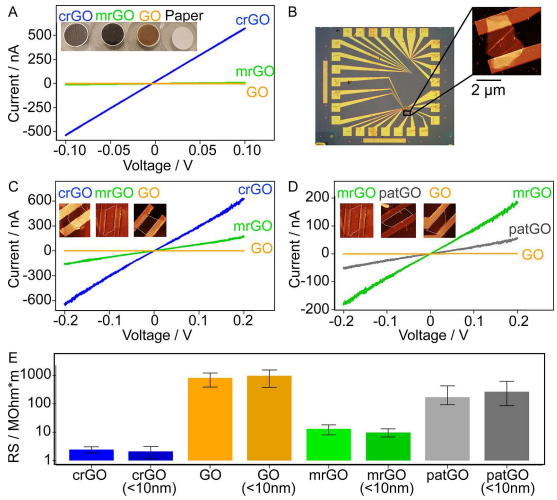

Figure 3. Resistance and patterning of microbially-reduced graphene oxide. (A) Bulk measurements of conductance performed on graphene oxide (orange), chemically-reduced graphene oxide (blue), and microbially-reduced graphene oxide (green) with a voltage bias of +/−0.1 V. The conductance increased by 3.2 orders of magnitude upon chemical reduction and by 2.1 orders of magnitude upon microbial reduction. Insets show bulk samples deposited onto filter paper. (B) Light microscopy and AFM image (inset) of a chip used to perform single-flake conductance measurements. (C) Conductance measurements of single flakes (shown in insets by AFM imaging) with comparable geometries at a voltage bias of +/−0.2 V. The conductance increased by 3.3 orders of magnitude upon chemical reduction (blue) and by 2.7 orders of magnitude upon microbial reduction (green). (D) Conductance measurements of microbially-reduced and microbially-patterned single flakes with comparable shapes (shown in insets by AFM imaging) at a voltage bias of +/−0.2 V. Patterned flakes (patGO, grey) were selectively reduced on only one side of the flake, resulting in an increase of conductance by 1.1 orders of magnitude. (E) The average sheet resistance determined for single-flake samples. The Rs value for GO (817 ± 423 MΩ) is 1.6 orders of magnitude higher than for mrGO flakes (13.2 ± 5.2 MΩ) and 2.3 orders of magnitude larger than for crGO (2.5 ± 0.6 MΩ) flakes. Measured flakes were divided into two groups based on the flake thicknesses: thickness between 10–100 nm, or thickness less than 10 nm (labelled "< 10 nm").

width ratio between 2.1 and 2.4) showed a 2.7 order-of-magnitude increase of the current at the same bias voltage for mrGO (55.32 S/m) relative to GO (0.11 S/m), and a 3.3 order-of-magnitude increase for crGO (216.56 S/m) relative to GO (0.11 S/m) (Figure 3C).

The data from the I–V curves and AFM analysis was used to calculate the sheet resistance (Rs) of GO, mrGO, and crGO (n = 11–18). These values are independent of the individual flake widths and lengths and are thus directly comparable. Rs was calculated using $Rs = R\,\frac{W}{L}$ with R the measured resistance, W width of the flake, and L its length or distance between the probes. The Rs value for GO (817 ± 423 MΩ) is 1.6 orders of magnitude higher than mrGO (13.2 ± 5.2 MΩ) and 2.3 orders of magnitude larger than crGO (2.5 ± 0.6 MΩ) flakes. To rule out the possibility that the resistance could be a function of the thickness, a population of flakes thinner than 10 nm (Figure 3E) was analysed. No significant differences were identified between the sheet resistances of single flakes that were thinner than 10 nm (GO: 972 ± 591 MΩ; mrGO: 9.9 ± 3.2 MΩ; crGO: 2.1 ± 0.9 MΩ) in comparison with single flakes from the same species with thicknesses between 10 and 100 nm (One-way ANOVA with Tukey PostHoc test, $p > 0.05$).

To generate patterned graphene oxide (patGO) flakes with only one reduced surface, GO was drop-casted onto a Si/SiO_2 chip. Afterwards, two layers of PMMA were spin-coated on top of the GO layer. E-beam lithography was used to create one to three windows per flake in the PMMA layer lying overtop of the GO flakes, with an average surface area of 25 μm^2. The exact dimensions and number of windows varied with the size of the flake. The windows were designed to allow bacteria to interact with the surface of the GO so that bacterial reduction could occur only on one side of the GO flake. These devices were microbially reduced with *S. oneidensis*, after which the conductance was determined in the same manner as for the single-flake conductance measurements. The conductance of patterned GO was 1.1 orders of magnitude larger than for GO (patGO:171 ± 265 MΩ), which is intermediate between the conductance increase of mrGO with respect to GO (Figure 3D, E). The microbially-reduced graphene oxide flakes were analyzed by AFM to detect any remaining adherent bacteria. After the final washing steps, only one out of eleven mrGO flakes showed a bacterium on its surface (Figure S2). In contrast, an average of ~2 bacteria per flake were identified in the AFM scans of the patterned GO flakes, likely due to the decreased amount of washing in this procedure (Figure S3).

2.3. Geometries of Microbially-Created Graphene Oxide Flakes

Aggregation of reduced graphene oxide materials over time can lead to a more graphite-like structure, negatively impacting their electrical and physical properties(39). To quantify the thickness distributions and surface area of the microbially-produced graphene oxide flakes, we performed AFM and light microscopy measurements of the graphene oxide samples (GO, mrGO, crGO). Half of the samples of a particular batch were measured immediately ("fresh" samples), and the other half were measured after two weeks of storage in water at room temperature ("stored" samples). Single flakes of GO, mrGO, and crGO were deposited onto a Si/SiO_2 chip using the same method as for the previous single-flake conductance measurements, and we compared their thicknesses via AFM measurements (Figure 4A).

When comparing the thicknesses of the stored vs. fresh samples, no significant differences were observed for either mrGO or GO (One-way ANOVA with Tukey PostHoc test, $p > 0.05$). However, the chemically-reduced GO flakes showed a significant change after storage, with a doubling of the average thickness (One-way ANOVA with Tukey PostHoc test, $p = 0.032$). When different GO materials were compared, the average thickness values for the fresh samples showed higher average values for crGO than for GO and mrGO, but the differences were not significant (crGO: 31.3 ± 7.0 nm; GO: 10.2 ± 0.4 nm; mrGO: 10.4 ± 0.4 nm). Among stored samples, the average thickness values for stored crGO flakes (56.4 ± 14.1 nm) were significantly higher than those of stored GO (10.4 ± 1.5 nm, p =

© 2019 The Authors. Published by Wiley-VCH Verlag GmbH & Co. KGaA

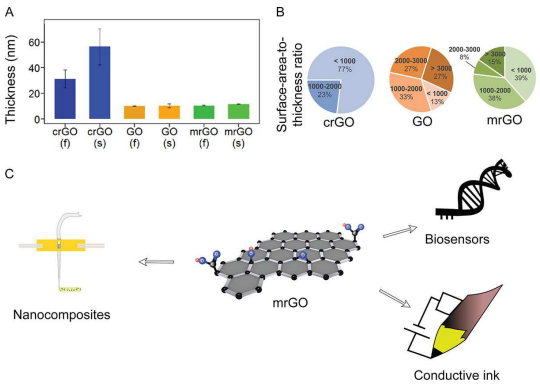

Figure 4. The thickness and surface-area-to-thickness ratio of mrGO flakes are key attributes for potential applications. (A) The average thickness of single flakes were determined via AFM. Graphene oxide(GO), microbially-reduced graphene oxide (mrGO), and chemically-reduced graphene oxide (crGO) were measured fresh ("f") and after a two-week storage ("s") in water. A significant difference was measured between the thicknesses of the crGO and the microbially-reduced and the GO flakes (mrGO: $p = 2e{-}6$, GO: $p = 2e{-}6$) as well as between the stored and fresh crGO flakes ($p = 0.32$) (One-way ANOVA with Tukey PostHoc test). (B) The surface-area-to-thickness ratio was determined for single flakes of GO, mrGO, and crGO and assigned to one of four groups (>3k:1,3k:1–2k:1, 2k:1–1k:1, <1k:1, with k equals 1000). (C) Proposed applications for mrGO based on its thickness and conductance properties. Biosensors are of interest because of the high surface-area-to-thickness ratio, the storability, and the remaining C=O double bonds which allow the possibility of chemical modifications. Nanocomposites could also benefit from the C=O double bonds as well as the feasibility of patterning, and the conductive ink industry could benefit from the conductivity combined with the improved storability in water as compared to chemically-reduced graphene oxide.

2e–6) and stored mrGO (11.6 ± 0.2 nm, $p = 2e{-}6$) (One-way ANOVA with Tukey PostHoc test).

Most applications favor graphene with minimal thickness (1–3 layers) and maximal surface area. This combination allows a transfer of the material's nanomaterial properties (high tensile strength, conductance) into macroscopic technology. To compare the surface-area-to-thickness proportionality of our mrGO samples, the surface area of individual flakes was determined via light microscopy imaging, and the thickness values obtained from AFM measurements. The calculated surface-area-to-thickness ratio for each flake was assigned to one of four groups (> 1000:1, 1000:1-2000:1, 2000:1-3000:1, > 3000:1) (Figure 4B). Graphene oxide showed the best distribution of surface-area-to-thickness ratios; 27% of the flakes had a ratio of over 3000:1, 27% had a ratio between 3000:1 and 2000:1, 33% of the flakes had a ratio between 2000:1 and 1000:1, and only 13% had a ratio below 1000:1. For mrGO, 15% of the flakes had a ratio higher than 3000:1; 8% had a ratio between 3000:1 and 2000:1, 38% had a ratio between 2000:1 to 1000:1, and 39% had a ratio below 1000:1. The proportion of high surface-area-to-thickness was the lowest for crGO, where no flakes showed a ratio above 2000:1. The ratio between 2000:1 to 1000:1 was only 23%, and a large majority of 77% was below 1000:1. The mean values for the surface-area-to-thickness showed a significant difference between crGO (707.88 ± 495.79 μm) and GO (2647.38 ± 485.51 μm) ($p = 0.0007$), but no significant differences were observed between GO and mrGO ($p = 0.0677$) or mrGO and crGO ($p = 0.1988$) (One-way ANOVA with Tukey PostHoc test, n = 13). Thus, overall mrGO flakes maintained lower thickness and higher surface-area-to-thickness ratios in comparison to crGO flakes.

3. Conclusions

This work is the first study to show the properties and applicability of microbially-reduced and -patterned graphene oxide with a focus on its conductance and surface-area-to-thickness ratio. *Shewanella oneidensis* was used as a model organism for microbial reduction, and we compared the microbially-produced mrGO to graphene oxide that was chemically reduced using hydrazine, the most popular method to produce rGO. Raman spectrometry, O.D. measurements, and XPS were used to determine the chemical and optical changes during the microbial and chemical reduction. AFM, SEM, and light microscopy revealed the flake dimensions in different reduction states. Conductivity measurements of bulk and single flakes allowed for an electrical characterization of our samples.

Analyses of the microbial reduction process under aerobic and anaerobic conditions confirmed that both conditions can allow for robust mrGO production (Figure 2C). The anaerobic process is more suitable for large-scale bioreactor applications since no oxygenation is needed, and it is more cost-efficient.[40] In contrast, the aerobic process is easier to handle on a smaller scale since no anaerobic equipment is required, and the samples may easily be transported.

The XPS and Raman measurements of differently-produced graphene oxide samples showed that chemical treatment with hydrazine removes almost all oxygen bonds from GO, while microbial reduction has little effect on the carbon-oxygen double bonds (Figure 2D, E). This comparison with the starting material (graphene oxide) allows a better understanding of the fundamental reduction capability of *Shewanella oneidensis*. We hypothesize that the higher bond energy of C=O in comparison to C-OH makes it unable to be reduced via the *Shewanella* reduction mechanism. Similarly, *Shewanella* is only able to utilize a limited set of inorganic terminal electron acceptors due to the moderate reduction capabilities of its electron-donating proteins and small molecules.[41] Microbial reduction of GO resulted in a 2.7 order-of-magnitude increase of conductance for single flakes of mrGO as well as an increase in conductance of 2.1 orders of magnitude in bulk mrGO samples (Figure 3A, C). Even though the conductivity of mrGO is lower than that measured for crGO, the presence of the C=O double bonds in mrGO may prevent additional π-π stacking of the rGO flakes, leading to the observation that the flake thickness seems to be better conserved upon mrGO production than for crGO production (Figure 4A). The production of smaller-thickness flakes for mrGO samples could be a significant advantage for applications that rely on a high surface-to-volume ratio.

Our experimental results showed that chemically-reduced flakes are more likely to form thicker aggregates than microbially-reduced flakes. In both fresh and stored samples, crGO flakes were thicker and had a worse surface-area-to-thickness ratio in comparison to GO and mrGO. Furthermore, the average

© 2019 The Authors. Published by Wiley-VCH Verlag GmbH & Co. KGaA

flake thickness of crGO samples increased significantly after a two-week storage period, which was not observed for either GO or mrGO samples. The increased amount of layers in chemically-reduced samples may be due to π-π stacking of crGO flakes occurring during the reduction process and continuing during storage. Thus, the high surface-area-to-thickness ratio and the improved storability of mrGO in comparison to crGO identifies mrGO as an effective material for applications requiring prolonged storage, such as conductive inks, biosensors, and materials for additive manufacturing.

The distinct chemical and conductive properties of mrGO in relation to crGO and GO indicate several promising application areas for mrGO (Figure 4C). The conservation of the carbon-oxygen double bonds in mrGO, shown through the XPS measurements, could be a valuable source for chemical modifications, which are necessary for most biosensors.[42] At the same time, the mrGO is up to 2.7 magnitudes more conductive than graphene oxide, which would enable applications requiring both chemical modification and electrical measurements (e.g. for field-effect transistor biosensors).[42,43] The lower proportion of carbon-oxygen single bonds in mrGO compared to GO could decrease the amount of accidentally-bound biomolecules during biosensing in comparison to GO and, therefore, increase the selectivity of biosensors made from mrGO in comparison to GO.[44] The improved storability of mrGO in water coupled with the 2.7 orders-of-magnitude increase in conductance may be beneficial for conductive inks as well. Finally, the possibility to spatially pattern mrGO flakes and the associated single-sided reduction would help to improve 3D-structural alignment in nanocomposites such as high-resolution bioprinting applications or composite (nano) materials, and could potentially be used for self-alignment of materials and sensors.[45]

Microbially-reduced graphene is distinguished from crGO by its improved surface-to-volume ratio (displayed via the surface-area-to-thickness ratio), better storability, the conservation of its carbon-oxygen double bonds, and a more sustainable production methodology, while having a comparable conductivity. Further improvement in the degree of reduction of mrGO could be possible through the use of a different metal-reducing bacteria strain, highlighting the importance of continuous efforts towards cultivating and characterizing environmental bacteria.[46,47] A direct improvement of the reductive behavior of *S. oneidensis* and its kinetics has also been achieved by increasing the number of electron shuttles, both by adding additional synthetic electron shuttles to the medium as well as by introducing genetic modifications to the bacterium itself to increase endogenous production of electron shuttle molecules.[26,48] All samples in this study were produced on a laboratory scale, and the next logical step towards economical feasibility would be upscaling in a bioreactor system. The upscaling of our methodology would allow a continuous process for the production of reduced GO to be initiated in bioreactors that would operate without the use of harsh chemistry or high energies. The results here obtained also indicate that the bacterial residues can be nearly completely washed away post-reduction. This approach would, therefore, be more sustainable and eco-friendly than the currently-used thermal or chemical methodologies, while maintaining the surface-to-volume ratio, which is critical for various applications of reduced graphene oxide.

Experimental Section

Bacterial Strains and Culturing

Shewanella oneidensis MR-1 (ATCC® 700550™) was aerobically and anaerobically cultured in rich Tryptic Soy Broth (TSB) media (Sigma Aldrich) or minimal media (28 mM NH_4Cl, 1.34 mM KCl, 5 mM NaH_2PO_4, 0.7 mM Na_2SO_4, 1 mM $MgSO_4$ $7H_2O$, 20 mM PIPES [piperazine-*N*,*N*′-bis(2-ethanesulfonic acid)], 52 mM NaCl, 0.2 mM $CaCl_2$, and trace elements (1 liter of medium contains 10 mg $FeCl_2$ $4H_2O$, 5 mg $MnCl_2$ $4H_2O$, 3 mg $CoCl_2$ $4H_2O$, 2 mg $ZnCl_2$, 0.5 mg Na_2MoO_4 $4H_2O$, 0.2 mg H_3BO_3, 1 mg $NiSO_4$ $6H_2O$, 0.02 mg $CuCl_2$ $2H_2O$, 0.06 mg Na_2SeO_3 $5H_2O$, and 0.08 mg Na_2WO_4 $2H_2O$) containing 20 mM L-lactate (Sigma Aldrich) and/or 20 mM Sodium fumarate dibasic (Sigma Aldrich) overnight at 30 °C under continuous shaking (250 rpm).[49]

Graphene Oxide Production

Graphite oxide was prepared using a modified Hummer and Offeman method[26, 46]. Briefly, 0.5 g graphite (pure graphite flakes with an average flake size of 45 μm (Ma −399.5 RG), NGS Trading & Consulting GmbH) was mixed with 20 mL H_2SO_4 (Sigma Aldrich) and 5 mL HNO_3 (Sigma Aldrich) under continuous stirring and on an ice bath. After 30 minutes of stirring, 3 g $KMnO_4$ (Sigma Aldrich) was added, after which the solution was stirred on an ice bath for 30 minutes, followed by incubation on the ice bath for one hour. The sample was heated to 35 °C for 3 hours and diluted with 40 mL ultrapure water, followed by an incubation at 35 °C for 2 hours. Then 100 mL ultrapure water was added. The graphite oxide solution was ultra-sonicated at 40 kHz (Carl Roth D30 ultrasonicator) for 2 hours and was allowed to settle overnight. The supernatant, now mainly consisting of graphene oxide, was decanted and washed with 5% HCl (Sigma Aldrich), acetone (Sigma Aldrich), and distilled water. Finally, the non-exfoliated flakes were removed via centrifugation (3000 rpm for 10 min), and the exfoliated flakes were lyophilized at −50 °C for 1 day (Christ Alpha 1–2 LD Plus lyophilizer).[50]

Chemical Reduction of Graphene Oxide

For the chemical conversion of graphene oxide to its reduced form, 30 mg of graphene oxide was dissolved in 100 mL distilled water and mixed vigorously. The sample was placed into a fume hood, and 120 μL hydrazine (35 wt% in H_2O, Sigma Aldrich) and 1 mL ammonia solution (28 wt% in H_2O, VWR International BV) were added. The solution was stirred at a temperature of 95 °C for 3 hours. Since the weight ratio of hydrazine to graphene oxide was 7:10, all hydrazine was used up during the reaction.[51]

Biological Reduction of Graphene Oxide

TSB medium including a concentration of 0.5 mg/mL graphene oxide was prepared and vigorously mixed. An overnight culture of *Shewanella oneidensis* MR-1 was diluted with this solution to an $O.D._{600}$ of 0.1. The reduction was performed aerobically or anaerobically for 48 hours under continuous shaking (250 rpm) at room temperature in a 96-well plate (Sigma Aldrich). The anaerobic

© 2019 The Authors. Published by Wiley-VCH Verlag GmbH & Co. KGaA

experiments were performed in anaerobic vessels (Sigma Aldrich) within a glove box (Plas Labs) and under nitrogen atmosphere. The growth of the bacteria was observed via measurement of optical density at 600 nm using a plate reader (Synergy HTX, Multimode reader).

Single-Flake Deposition and Inspection

A volume of 0.25 mL graphene oxide flakes, microbially-reduced graphene oxide flakes, or chemically-reduced graphene oxide flakes with a concentration of 0.1 mg/mL in water was drop-casted onto a Si/SiO_2 (285 nm SiO_2) device (Microchemicals) with premade gold markers. The residual solvent was washed away with acetone and isopropanol for all samples. The devices were inspected for sufficient sample deposition under an optical microscope (Olympus BX 5, with DP25 camera), and images were acquired of samples. After alignment of the images using QCAD® software, electrical leads were drawn onto selected flakes via the following procedure. Two layers of PMMA (PMMA A6 495 K followed by PMMA A3 950 K) were sequentially spin-coated onto the surface of the device at 4500 rpm and baked for 12 minutes at 175 °C. The CAD file was uploaded to and patterned with an e-beam system (Raith EBPG 5000+), and layers of titanium (5 nm) and gold (75 nm) were evaporated onto the surface using an e-gun for metal evaporation of metals (Temescal FC2000). The PMMA was lifted off in hot acetone (80 °C), and an isopropanol washing step was performed. The device was inspected again under the optical microscope to check for lost flakes or improperly drawn leads prior to conductance measurement. After conductance measurements, the graphene oxide flakes were inspected again via optical microscopy as well as via a scanning electron microscope (FEI NovaNanoSEM) using 5–15 kV voltage and 5 mm working distance.

Single Flake Conductance Measurements

A probe station (TTP4 Desert, Lakeshore)_was used to measure a varying voltage bias (+/−0.2 V) applied to GO, mrGO, crGO, and patGO samples. The current as a function of the voltage bias was recorded and used to calculate the resistance of individual flakes over a set of distances (R (resistance) = V (voltage)/I (current)). AFM measurements (AFM Dimension FastScan, Brucker, tapping mode in air, fast-scan tip) were taken of the outer dimensions and the thickness of the single flakes to determine the size distribution of the flakes and calculate the intrinsic resistivity (ρ (resistivity) = R (resistance)*A (area)/L (length)) and sheet resistance (R_S (sheet resistance) = R (resistance) * W (width)/L (length)).

Bulk Conductance Measurement

Graphite, graphene oxide, microbially-reduced graphene oxide, and chemically-reduced graphene oxide were prepared, and 15 mL of a 0.5 mg/mL solution of each sample was vacuum filtered (Vacuum Filtration Unit Buchner Medium 60 mL Frit Funnel 250 mL Erlenmeyer Flask) through a 0.2 μm PTFE filter (Whatman, PTFE membrane filters). The deposited material was rinsed once in a 10% solution of HCl and 5 times in MilliQ water. Thereafter, the filter paper was air-dried, and conductance was measured over its full diameter using a probe station (TTP4 Desert, Lakeshore).

Bacterial Lithography

Graphene oxide was deposited via drop casting onto a Si/SiO_2 device (Microchemicals). Suitable flakes (high surface area low thickness) were inspected and selected under an optical microscope (Olympus BX 5, with DP25 camera). Two layers of PMMA were spin-coated onto the surface of the device. QCAD® software was used to design windows (dimensions 5×5 μm^2) in the PMMA layers, which were cut out via an e-beam system (Raith EBPG 5000+). After five washing steps in distilled water, the devices were placed into a *Shewanella* solution with a starting $O.D._{600}$ of 0.1. The devices were incubated in the solution for 48 hours at room temperature. The conductance was measured following the method for single-flake conductance measurements.

X-Ray Photoelectron Spectroscopy (XPS)

X-ray photoelectron (XPS) spectra were recorded on a ThermoFisher K-Alpha system using Al Kα radiation with a photon energy of 1486.7 eV. The samples were immobilized onto a copper tape (Plano GmbH, G3397) and loaded into the XPS chamber without further purification. High-resolution XPS spectra were acquired using a spot size of 400 μm, 50 eV pass energy, and 0.1 step size, with 40 scans (for carbon and nitrogen spectra) or 10 scans (for oxygen spectrum) with charge neutralizing. The peaks were calibrated for the C 1s peak at 285 eV. Quantitative analysis of the separate binding states was carried out by deconvoluting the high-resolution spectra using ThermoFisher Advantaged software. Gaussian-Lorentzian product functions were used to fit the peaks after Smart-type background subtraction. The chemical bond ratios were then calculated by correcting the peak areas with the TPP-2 M sensitivity factor. All fits that occurred in both spectra were cross-checked to verify their fit-match.

Statistics

R-Studio was used for data analysis and visualisation. All datasets were checked for outliers with a Dixon's Q-Test. Unless noted, no outliers were removed from the datasets. The variance was tested using an F-test, and Student's t-test with either equal or unequal variances was used for comparing two data sets, with a significance level of $\alpha = 0.05$. We used a one-way ANOVA with Tukey PostHoc Test to compare more than two datasets.

Surface-Area-to-Thickness ratio

X-ray photoelectron For analysis of the surface-area-to-thickness ratios of individual flakes, flakes were separated into four distinct groups (<1000:1, 1000:1–2000:1, 2000:1–3000:1, >3000:1). The surface area was measured from SEM images using ImageJ and divided by the average thickness obtained from the AFM to calculate the ratio.

Colony Forming Units (CFU) to Check the Bacterial Survival Rate

Colony forming units (CFU) were determined following the protocol of Karas et al.[52] In short, each sample was serially diluted in ten-fold increments from 10–0 to 10–7. A volume of 5 μL from each dilution was pipetted in triplicates onto a LB agar plate. The plates were incubated at 22 °C for 24 hours, and visible colonies were counted.

Acknowledgements

Our thanks to Carsten Blom and Bertus Beaumont for their assistance in anaerobic work and to Filipe Natalio, Wayne Yang,

© 2019 The Authors. Published by Wiley-VCH Verlag GmbH & Co. KGaA

and Allard Catan for their help with Raman, AFM, and SEM measurements. This work was supported by the Netherlands Organization for Scientific Research (NWO/OCW), as part of the Frontiers of Nanoscience program.

Conflict of Interest

The authors declare no conflict of interest.

Keywords: microbial reductions · sustainable reactions · graphene oxide · *Shewanella oneidensis* · nanomaterials

[1] K. S. Novoselov, A. K. Geim, S. V. Morozov, D. Jiang, Y. Zhang, S. V. Dubonos, I. V. Grigorieva, A. A. Firsov, *Science* **2004**, *306*, 666–669
[2] R. Kumar, B. R. Mehta, M. Bhatnagar, S. Mahapatra, S. Salkalachen, P. Jhawar, *Nanoscale Res. Lett.* **2014**, *9*, 349
[3] B. Marinho, M. Ghislandi, E. Tkalya, C. E. Koning, G. de With, *Powder Technol.* **2012**, *221*, 351–358
[4] A. A. Balandin, S. Ghosh, W. Bao, I. Calizo, D. Teweldebrhan, F. Miao, C. N. Lau, *Nano Lett.* **2008**, *8*, 902–907
[5] C. Lee, X. Wei, J. W. Kysar, J. Hone, *Science* **2008**, *321*, 385–388
[6] X. Zhu, J. Li, H. He, M. Huang, X. Zhang, S. Wang, *Biosens. Bioelectron.* **2015**, *74*, 113–133
[7] S. Shi, W. Jiang, T. Zhao, K. E. Aifantis, H. Wang, L. Lin, Y. Fan, Q. Feng, F. Z. Cui, X. Li, *J. Biomed. Mater. Res.* **2015**, *103*, 3978–3992
[8] V. Palermo, I. A. Kinloch, S. Ligi, N. M. Pugno, *Adv. Mater.* **2016**, *28*, 6232–6238
[9] A. D Franklin, *Science* **2015**, *349*, 2750
[10] J. S. Chen, X. W. Lou, *Small* **2013**, *9*, 1877–1893
[11] G. K. Dimitrakakis, E. Tylianakis, G. E. Froudakis, *Nano Lett.* **2008**, *8*, 3166–3170
[12] Y. Liu, H. Cai, F. Wang, J. Wang, Q. Huang, Z. Fu, Y. Lu, *Nanoscale* **2018**, *8*
[13] L. Rodriguez-Perez, M. A. Herranz, N. Martin, *Chem. Commun.* **2013**, *49*, 3721–3735
[14] D. R. Dreyer, S. Park, C. W. Bielawski, R. S. Ruoff, *Chem. Soc. Rev.* **2010**, *39*, 228–240
[15] P. T. Araujo, M. Terrones, M. S. Dresselhaus, *Mater. Today* **2012**, *15*, 98–109
[16] Y. Zhang, L. Zhang, C. Zhou, *Acc. Chem. Res.* **2013**, *46*, 2329–2339
[17] B. Chen, H. Huang, X. Ma, L. Huang, Z. Zhang, L. M. Peng, *Nanoscale* **2014**, *6*, 15255–15261
[18] S. Abdolhosseinzadeh, H. Asgharzadeh, H. Seop Kim, *Sci. Rep.* **2015**, *5*, 10160
[19] J. H. William, R. E. Offeman, *J. Am. Chem. Soc.* **1958**, *80*, 1339
[20] I. K. Moon, J. Lee, R. S. Ruoff, H. Lee, *Nat. Commun.* **2010**, *1*, 73
[21] D. C. Marcano, D. V. Kosynkin, J. M. Berlin, A. Sinitskii, Z. Sun, A. Slesarev, L. B. Alemany, W. Lu, J. M. Tour, *ACS Nano* **2010**, *4*, 4806–4814
[22] C. K. Chua, M. Pumera, *Chem. Soc. Rev.* **2014**, *43*, 291–312
[23] H. C. Schniepp, J. L. Li, M. J. McAllister, H. Sai, M. Herrera-Alonso, D. H. Adamson, R. K. Prud'homme, R. Car, D. A. Saville, I. A. Aksay, *J. Phys. Chem. B* **2006**, *110*, 8535–8539
[24] E. C. Salas, Z. Sun, A. Luttge, J. M. Tour, *ACS Nano* **2010**, *4*, 4852–4856
[25] Y. Jiao, F. Qian, Y. Li, G. Wang, C. W. Saltikov, J. A. Gralnick, *J. Bacteriol.* **2011**, *193*, 3662–3665
[26] G. Liu, X. Zhang, J. Zhou, A. Wang, J. Wang, R. Jin, H. Lv, *Bioresour. Technol.* **2013**, *149*, 503–508
[27] G. Fan, C. M. Dundas, A. J. Graham, N. A. Lynd, B. K. Keitz, *Proc. Natl. Acad. Sci. USA* **2018**, *115*, 4559
[28] P. Bollella, G. Fusco, C. Tortolini, G. Sanzo, G. Favero, L. Gorton, R. Antiochia, *Biosens. Bioelectron.* **2017**, *89*, 152–166
[29] M. Zhou, Y. Zhai, S. Dong, *Anal. Chem.* **2009**, *81*, 5603–5613
[30] S. Pei, H. M. Cheng, *Carbon* **2012**, *50*, 3210–3228
[31] K. S. Novoselov, V. I. Fal'ko, L. Colombo, P. R. Gellert, M. G. Schwab, K. Kim, *Nature* **2012**, *490*, 192
[32] L. Huang, Y. Huang, J. Liang, X. Wan, Y. Chen, *Nano Res.* **2011**, *4*, 675–684
[33] L. Y. Xu, G. Y. Yang, H. Y. Jing, J. Wei, Y. D. Han, *Nanotechnology* **2014**, *25*, 055201
[34] Y. Talukdar, J. Rashkow, G. Lalwani, S. Kanakia, B. Sitharaman, *Biomaterials* **2014**, *35*, 4863–4877
[35] G. Lalwani, W. Xing, B. Sitharaman, *J. Mater. Chem. B.* **2014**, *7*, 6354–6362
[36] H. J. Kim, S. M. Lee, Y. S. Oh, Y. H. Yang, Y. S. Lim, D. H. Yoon, C. Lee, J. Y. Kim, R. S. Ruoff, *Sci. Rep.* **2014**, *4*, 5176
[37] D. Yang, A. Velamakanni, G. Bozoklu, S. Park, M. Stoller, R. D. Piner, S. Stankovich, I. Jung, D. A. Field, C. A. Ventrice Jr, R. S. Ruoff, *Carbon* **2009**, *47*, 145–152
[38] A. C. Ferrari, D. M. Basko, *Nat. Nanotechnol.* **2013**, *8*, 235–246
[39] I. Chowdhury, N. D. Mansukhani, L. M. Guiney, M. C. Hersam, D. Bouchard, *Environ. Sci. Technol.* **2015**, *49*, 10886–10893
[40] A. Abdelgadir, X. Chen, J. Liu, X. Xie, J. Zhang, H. Wang, N. Liu, *BioMed Res. Int.* **2014**, *841573*
[41] C. R. Myers, K. H. Nealson, *Science* **1988**, *240*, 1319
[42] Q. Zhang, D. Zhang, Y. Lu, Y. Yao, S. Li, Q. Liu, *Biosens. Bioelectron.* **2015**, *68*, 494–499
[43] E. Masoudipour, S. Kashanian, N. Maleki, A. Karamyan, K. Omidfar, *Drug Dev. Ind. Pharm.* **2018**, *44*, 99–108
[44] J. Liu, Z. Liu, C. J. Barrow, W. Yang, *Anal. Chim. Acta.* **2015**, 859, 1–19
[45] B. A. E. Lehner, D. T. Schmieden, A. S. Meyer, *ACS Synth. Biol.* **2017**, *6*, 1124–1130
[46] G. Wang, F. Qian, C. W. Saltikov, Y. Jiao, Y. Li, *Nano Res.* **2011**, *4*, 563–570
[47] J. E. Kostka, D. D. Dalton, H. Skelton, S. Dollhopf, J. W. Stucki, *Appl. Environ. Microbiol.* **2002**, *68*, 6256
[48] Y. Yang, Y. Ding, Y. Hu, B. Cao, S. A. Rice, S. Kjelleberg, H. Song, *ACS Synth. Biol.* **2015**, *4*, 815–823
[49] Y. J. Tang, D. Laidlaw, K. Gani, J. D. Keasling, *Biotechnol. Bioeng.* **2006**, *95*, 176–184
[50] G. Lee, B. S. Kim, *Biotechnol. Prog.* **2014**, *30*, 463–469
[51] D. Li, M. B. Muller, S. Gilje, R. B. Kaner, G. G. Wallace, *Nat. Nanotechnol.* **2008**, *3*, 101–105
[52] V. O. Karas, I. Westerlaken, A. S. Meyer, *J. Bacteriol.* **2015**, *197*, 3206–3215

Manuscript received: May 29, 2019

© 2019 The Authors. Published by Wiley-VCH Verlag GmbH & Co. KGaA